Available online at www.sciencedirect.com
SCIENCE DIRECT®
Journal of Molecular Catalysis A: Chemical 225 (2005) 39–46
JOURNAL OF MOLECULAR CATALYSIS A: CHEMICAL
www.elsevier.com/locate/molcata

Characterization of sulfated TiO_2 prepared by the sol–gel method and its catalytic activity in the *n*-hexane isomerization reaction

Lúcia K. Noda*, Rusiene M. de Almeida, Luiz Fernando D. Probst, Norberto S. Gonçalves

Departamento de Química, Laboratório de Catálise Heterogênea, Universidade Federal de Santa Catarina, Florianópolis CEP 88040-900, SC, Brazil

Received 20 May 2004; received in revised form 23 August 2004; accepted 23 August 2004
Available online 2 October 2004

Abstract

Sulfated TiO_2 was prepared by a single-step sol–gel method, in which the hydrolysis and sulfation occur in the same step, varying some conditions of the preparation method. The characterization was carried out by thermogravimetric analysis, infrared absorption spectroscopy, Raman spectroscopy, pyridine adsorption infrared spectroscopy for the determination of the Brönsted acid sites/Lewis acid sites ratio, determination of the specific surface area (BET method), average pore diameter (BJH method) and catalytic activity in the *n*-hexane isomerization reaction.

In the infrared spectra it was verified that the sulfate is coordinated to the titanium in a chelate form, while in the Raman spectra it was observed that the samples are in an anatase crystalline form.

Catalytic tests of the *n*-hexane conversion at 100 and 200 °C were carried out. At 100 °C, it was observed that the selectivity for isomerization and catalytic stability are higher than at 200 °C, however, at 100 °C the conversion is lower than at 200 °C.

Among the structural and textural properties investigated, it was found that the samples which had greater average pore diameters and a higher Brönsted acid sites/Lewis acid sites ratio were the ones which showed greater catalytic activity.

Keywords: TiO_2; Sulfate; *n*-Hexane; Isomerization; Brönsted and Lewis acid sites

1. Introduction

Solid acid catalysts form the greater part of catalysts used in petroleum refining and in the petrochemical industry. They are used in conversion reactions of hydrocarbons derived from petroleum, such as alkylation, isomerization, cracking, etc. Some examples of these catalysts are silica–alumina, aluminophosphates, silica–alumina–phosphates, zeolites, heteropolyacids and metallic sulfate oxides [1].

In some types of reactions, such as alkane isomerization, a great problem which is faced with conventional solid acid catalysts is the low selectivity, due to the high temperature needed for carrying out the reactions, which ends up provoking secondary reactions. In order to overcome this problem many studies have been recently carried out to find highly acidic solids which can be used at lower temperatures, hence being more selective.

Sulfated metallic oxides are examples of highly acidic solids, classified by some authors as superacids [2]. Hino and co-workers initially investigated sulfated ZrO_2 and TiO_2, with which it was possible to carry out *n*-butane isomerization at ambient temperature [3,4]. The isomerization of alkanes at ambient temperature is of interest to the petroleum industry since ramified alkanes are important for generating products which increase the octane number of gasoline. The reaction at ambient temperature represents not only an economy of energy, but also favors, thermodynamically, the ramified products [5].

* Corresponding author. Tel.: +55 48 331 92 19; fax: +55 48 331 97 11.
E-mail address: lucia@qmc.ufsc.br (L.K. Noda).

1381-1169/$ – see front matter © 2004 Elsevier B.V. All rights reserved.
doi:10.1016/j.molcata.2004.08.025

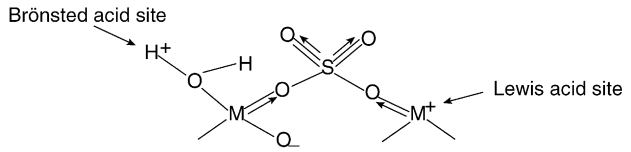

Scheme 1. Brönsted and Lewis acid sites in sulfated metal oxide.

In the sulfated metallic oxides there may be as many Lewis acid sites as Brönsted acid sites. The superacidity of these materials is attributed to the Brönsted acid sites, created or already existing, whose acidity is increased by the presence of neighboring strong Lewis acid sites. The strength of these Lewis acid sites is due to an inductive effect exercised by sulfate on the metallic cation, which becomes more deficient in electrons, as seen in the Scheme 1.

It was found that Brönsted acidity is very important to the catalytic activity of sulfated ZrO_2 [6,7] and of sulfated TiO_2 [8]. The Brönsted acid sites would be formed in samples with higher sulfate content [6,7,9,10] in which the sulfate would have a polynuclear structure [7]. The experimental factors which influence the formation of the Brönsted and Lewis acid sites are the preparation method, the sulfate content, and the calcination temperature.

The first preparations of sulfated metallic oxides were carried out through the impregnation of TiO_2, previously prepared, with H_2SO_4 or $(NH_4)_2SO_4$ [11]. However, Farcasiu and Li [12] observed that it was not possible to control the quantity of sulfate groups through the impregnation method. Ward and Ko [13] found an effective way to prepare the sulfated ZrO_2, in a singe step, using the sol–gel method, thus controlling the quantity of sulfate. According to this method, an H_2SO_4 solution in water was added to zirconium alkoxide, in the gel formation stage. Armendariz et al. [14] also prepared sulfated ZrO_2 by the sol–gel method, with aqueous H_2SO_4 being added to zirconium alkoxide, as in the Ward and Ko preparation, or only concentrated H_2SO_4 was added to the alkoxide in the pre-hydrolysis period, later adding water to carry out the hydrolysis.

It was found that when H_2SO_4 is added to zirconium alkoxide in the pre-hydrolysis stage, the sulfated ZrO_2 obtained has larger pores than in that obtained with the addition of H_2SO_4 in the hydrolysis stage. Textural properties, such as surface area and average pore diameter play an important role in heterogenic catalysis [15], such as in reagent conversion and in selectivity for the desired products.

The number of studies involving the preparation, characterization and utilization of sulfated ZrO_2 in various reactions which need sites of high acidity, is very high. However, studies involving sulfated TiO_2, which also has superacidity characteristics, are more scarce. The utilization of catalysts based on TiO_2 is of great economic interest in some countries with large reserves of titanium oxide or mineriums like ilmenite ($FeTiO_3$), from which it is possible to obtain TiO_2.

The characterization of catalysts may be carried out through structural, electric, magnetic, textural and morphological properties, etc.

The structure of catalysts, including the study of the interaction with adsorbed molecules, can be investigated through spectroscopic methods involving electronic, vibrational and spin (nuclear and electronic) transitions [16,17].

Infrared absorption spectroscopy is frequently used for the determination of acid sites at surfaces, employing probe molecules, which have characteristic vibrational frequencies, depending on the type of site in which they are adosorbed, that is, in Brönsted or Lewis acid sites.

Raman spectroscopy is particularly useful for the characterization of catalysts in the low frequency region, which is the region where the majority of catalysts are opaque in the infrared spectrum, due to the very intense absorption of metallic oxides, used as catalysts or supports, which are, however, weak Raman scatterers [17]. For instance, TiO_2 has Raman spectra very characteristic of anatase, rutile and brookite crystalline forms, which does not occur with infrared spectra. Further, it is possible to employ Raman spectroscopy to investigate species adsorbed on catalyst surfaces, as reported in a previous work concerning styrene oligomers on TiO_2 surface [18,19].

Textural properties such as specific surface area and average pore diameter may be determined utilizing the methods described by Brunauer–Emmett–Teller and Barrett, Joyner and Halenda [20].

This study aims towards the preparation and characterization of sulfated TiO_2 by the sol–gel method and the measurement of catalytic activity in a reaction which requires very strong acid sites, such as *n*-hexane isomerization. The correlation between the properties of sulfated TiO_2, such as type of acid sites, crystalline form, sulfate group stability, surface area, pore diameter and its catalytic activity will be investigated.

2. Experimental

2.1. Preparation of sulfated TiO_2 by the sol–gel method

Samples were prepared by the sol–gel method, in a single step, that is, the sulfatating agent, in this case H_2SO_4, was added in the hydrolysis or the pre-hydrolysis stage. Some conditions were varied, as described below.

Sample 1: To a solution of *iso*-propanol (*i*-PrOH) and titanium *iso*-propoxide (Ti(*i*-PrO)$_4$), 1.0 mL of H_2SO_4 3.6 mol L^{-1} was added while shaking. The gel formed was left to stand for 1.5 h. The alcohol was evaporated and the resulting product was dried at 150 °C for 12 h. The solid was calcined at 390 °C for 5 h.

Sample 2: The same procedure used for sample 1 was utilized, however, 0.2 mL of concentrated H_2SO_4 was first added, followed by 0.8 mL of H_2O. Thus, the quantities of

H_2SO_4 and H_2O added, in moles, are equal to those of preparation 1.

Sample 3: In this procedure the hydrolysis is carried out in an aqueous solution of HNO_3 and H_2SO_4, and not only H_2SO_4, as in the two previous procedures. To a solution of Ti(*i*-PrO)$_4$ in *i*-PrOH, 1.5 mL of HNO_3 70% (v/v) was added, followed by 0.4 mL of concentrated H_2SO_4 while shaking. A solution of *i*-PrOH/H_2O to bring about the hydrolysis was then added. After the gel formation, it was left to stand for 1.5 h, the alcohol was evaporated and the product was dried at 150 °C for 12 h.

Sample 3a consisted simply of sample 3 calcined at 300 °C for 10 h. The color of the samples varied from white to light beige.

2.2. Thermogravimetric analysis

The thermogravimetric analyses were carried out with a Shimadzu TGA-50 instrument, under nitrogen atmosphere, within the temperature range 25–900 °C, with a heating rate of 10 °C/min.

2.3. Infrared spectroscopy

2.3.1. Sulfated TiO_2 spectra

The spectra were obtained with a Perkin-Elmer System 2000 spectrometer, with the sample diluted in KBr pellets.

2.3.2. Spectra of pyridine adsorbed on sulfated TiO_2

The spectra were obtained by diffuse reflectance, with a Bomem DA3.16 FTIR spectrometer, using a Spectra-Tech catalytic cell, which allows heating, the creation of a vacuum and the introduction of the vapor of the substance under study. The procedure for the sample activation and obtention of spectra is described as follows. The sulfated TiO_2, in the form of a powder, slightly compacted, was previously heated to 100 °C for 30 min, then to 200 °C for 30 min and finally to 300 °C for 30 min in the catalytic cell with an oxygen flow. After this period, under vacuum, the temperature of the cell was reduced to 100 °C. The pyridine vapor was introduced into the cell at 100 °C, leaving the entrance valve open for around 3 min, after creating a vacuum to remove the pyridine excess. After the removal of excess pyridine the infrared spectrum was recorded at a temperature of 100 °C, increasing the temperature to 200 °C and then 300 °C, recording the spectra at each of these temperatures. The spectra were acquired in the form of raw reflectance data.

2.4. Raman spectra

The Raman spectra were obtained with a Renishaw System 3000 instrument, using as the source of excitation the 632.8 nm line of a He–Ne laser (Spectra Physics). The samples were in compacted powder form, without dilution.

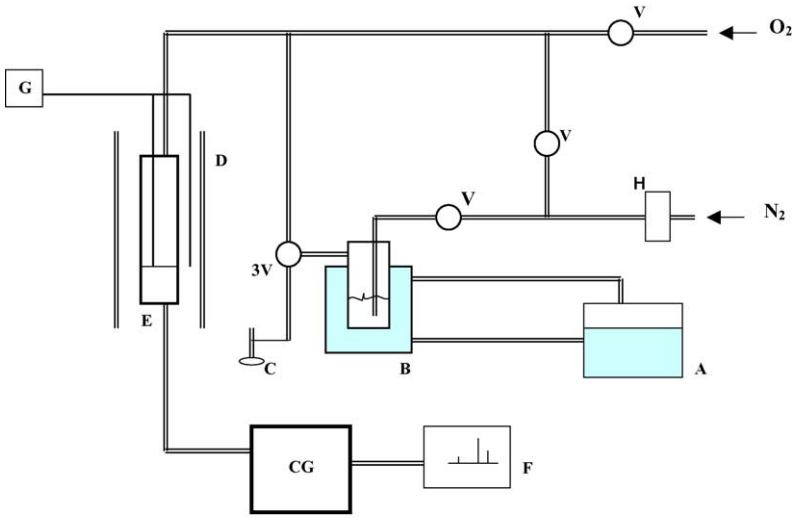

A – Thermostated bath; **G** – Thermocouple;
B – Saturator; **H** – Molecular sieve;
C – Flow meter; **CG** – Chromatograph;
D – Oven; **3V** – 3-way valve;
E – Reactor; **V** – Simple valve;
F – Recorder;

Fig. 1. Schematic representation of the reaction line.

2.5. Specific surface area and average pore diameter

The analyses of the surface areas and average pore diameters were carried out with an Autosorb-1-C (Quantachrome Corporation) instrument. The samples were previously activated at 200 °C under vacuum for 2 h, and the analyses of the physical adsorption/desorption of N_2 at 77 K was then carried out.

The specific surface areas were determined through the isothermal model of Brunauer–Emmett–Teller (BET). For the calculation of the average pore diameters the Barret, Joyner and Hallenda (BJH) method was used, which consists of determining the distribution of the pore diameters of the sample.

2.6. Catalytic tests

The reactions were carried out with the reagent in the gaseous phase, under continuous flow, utilizing nitrogen as the diluent gas. The products were analyzed with a Shimadzu GC-14B chromatograph, with an apolar capillary column (CBP1) and a flame ionization detector. A metal reaction system was utilized, as shown in Fig. 1, with an internal diameter of around 3 mm and a glass U-shaped reactor.

One hundred milligram of the sample were heated to 300 °C for a period of 3 h under oxygen flow. The heater was switched off and left to reach the desired value, the oxygen flow was removed and the nitrogen/*n*-hexane mixture flow was then introduced. The *m*/*F* ratio (*m* is the catalyst mass in grams and *F* the flow of *n*-hexane in mol/min) was 5.7×10^3 g min mol^{-1}. The reaction was carried out at two temperatures, 100 and 200 °C.

3. Results and discussion

3.1. Thermogravimetric analysis

In the weight loss and first derivative curves (Fig. 2) the weight loss of water in the temperature range 80–200 °C and the weight loss of sulfate at temperatures above 400 °C, are observed.

On analyzing the first derivative curves in the region of sulfate loss, two samples with only a peak of sulfate loss below 600 °C are observed, while another sample had two peaks above 600 °C and one sample had one peak above 600 °C and another peak below 600 °C (Table 1). Ward and Ko [13] also observed for sulfated ZrO_2 prepared by the sol–gel method that some samples had different regions of sulfate loss, the lowest temperature peak being attributed to a more weakly bound sulfate species, whereas the highest temperature peak was attributed to a more strongly bound sulfate. In a recent study [8] we found that sulfated TiO_2 shows the same behavior, that is, there were distinct ranges of sulfate loss temperature which corresponded to the sulfates bound to different

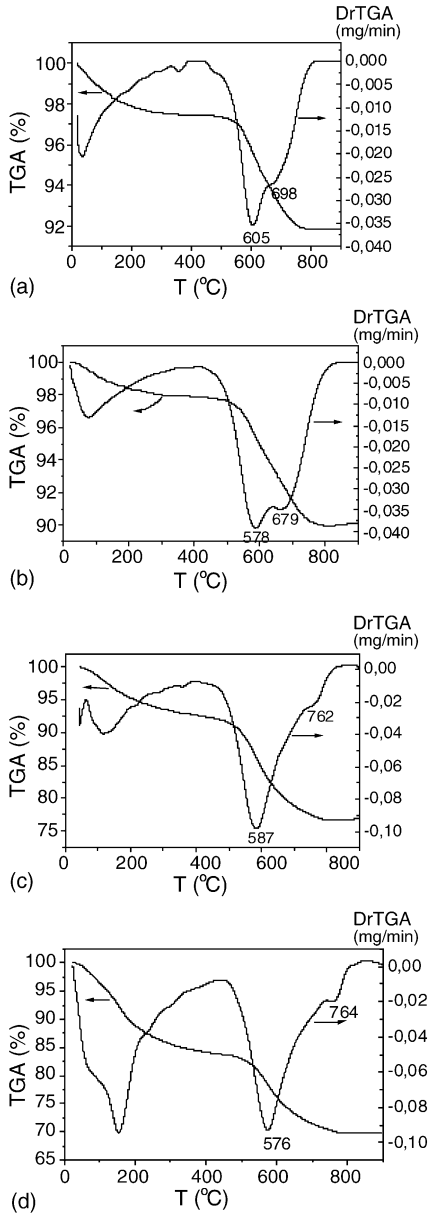

Fig. 2. Thermograms (TGA) and first derivative curves (DTGA) of samples: (a) 1; (b) 2; (c) 3; (d) 3a.

Table 1
Weight loss of sulfate (%) from the thermogravimetric analyses

Sample	*T* (°C)	SO_4 (wt.%)
1	605	3.4
	698	2.2
2	579	4.1
	679	3.7
3	576	14.0
3a	587	15.5

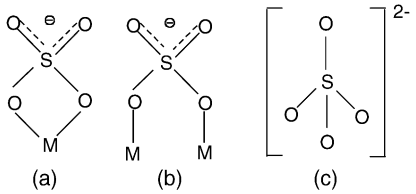

Fig. 3. Sulfate structures: (a) coordinated, C_{2v} (chelate) and (b) coordinated, C_{2v} (bridge) and (c) free sulfate (T_d).

types of acid sites.

3.2. Infrared absorption spectra

3.2.1. Sulfated TiO_2

In the sulfated metal oxides, the sulfate is covalently bound to the oxide, there being changes in its structure, which reflects in their vibrational spectra.

The free sulfate ion has T_d symmetry (Fig. 3(c)), with a very intense band in the infrared spectrum at around 1100 cm^{-1} (ν_3 mode). For salts in the solid state there is a splitting of the degenerated modes, due to the reduction in symmetry, such as ν_3, which are split into three components between 1100 and 1170 cm^{-1}, and also previously inactive modes may become active, such as ν_1 which may appear very weakly at 990–1020 cm^{-1} [21].

The sulfate coordinated to metals may have C_{2v} symmetry, when bound by two oxygens, it being that in this case there may be two types of coordination, such as the chelate (a) and the bridge (b) complexes, shown as follows.

The infrared absorption spectra of the samples (Fig. 4) show bands between 1300 and 990 cm^{-1}, which are attributed to the sulfate vibrational modes. Only the spectra of samples 1 and 2 are shown since the other sample spectra are practically the same.

A band at around 1220–1235 cm^{-1} present for all samples is attributed to asymmetric stretching of the S=O bond and the band at around 1130 cm^{-1} to the symmetric stretching of the S=O bond. The band at around 1040 cm^{-1} is attributed to the asymmetric S–O bond. Samples 3 and 3a show a band at around 980 cm^{-1} relating to the symmetric stretching of the S–O bond. All of these bands are related to the sulfate bound to the metal oxide in the chelate form.

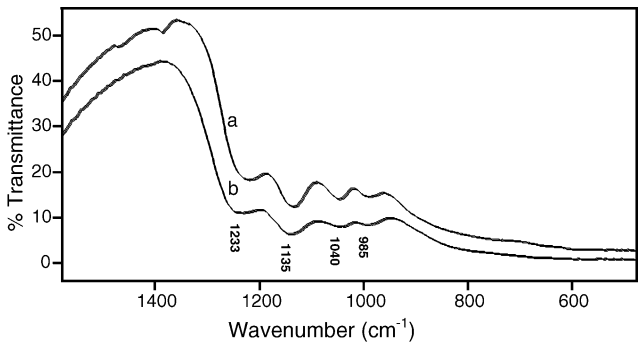

Fig. 4. Infrared spectra of sulfated TiO_2: (a) sample 3 and (b) sample 3a.

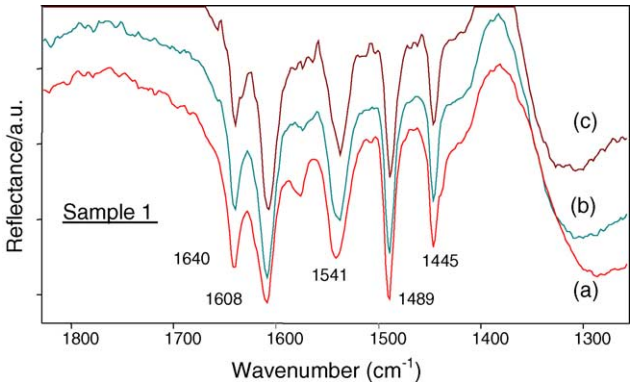

Fig. 5. Corrected infrared spectra of sample 1, after the introduction of pyridine at: (a) 100 °C; (b) 200 °C and (c) 300 °C in the catalytic cell.

3.2.2. Pyridine adsorbed on sulfated TiO_2

The infrared spectra of pyridine adsorbed on sulfated TiO_2 (sample 1) at 100, 200 and 300 °C, are shown in Fig. 5. The raw reflectance spectra were corrected in order to eliminate the rotational bands of water, present in the original spectra. The spectrum of sulfated TiO_2 before the adsorption of pyridine was subtracted from the spectrum of the sulfated TiO_2/pyridine. The spectral subtraction was carried out with the Grams 386 program.

Frequencies at around 1635, 1609, 1539, 1487 and 1447 cm^{-1} are observed in the spectra, which are characteristic of pyridine adsorbed in acid sites. In Table 2, the frequencies of adsorbed pyridine, together with the respective assignment [1] (Lewis and/or Brönsted acid sites) are shown.

The proportion of Brönsted to Lewis acid sites can be found from the relative intensity between the bands at 1540 cm^{-1} and at around 1450 cm^{-1}, which are due to the Brönsted and Lewis acid sites, respectively. In Table 3 the ratio of Brönsted acid sites/Lewis acid sites are shown, with the intensities of the bands measured from their height. It can be seen that samples 2 and 3a showed a higher ratio of Brönsted acid sites/Lewis acid sites. It can also be seen that acid sites are strong, since the pyridine is not desorbed even at higher temperatures.

3.3. Raman spectra

The Raman spectra of sulfated TiO_2 (Fig. 6) are characteristic of the anatase crystalline form, with bands at 402–409, 513–518 and 633–645 cm^{-1}. This crystalline form presents greater catalytic activity for various reactions, due to the pres-

Table 2
Infrared frequencies of pyridine adsorbed on the Lewis and Brönsted acid sites

Sample	Coordinated pyridine (Lewis acid site) (cm^{-1})			Pyridine ion (Brönsted acid site) (cm^{-1})	
1	1446	1488	1607	1539	1636
2	1447	1487	1609	1539	1635
3	1447	1488	1609	1541	1635
3a	1446	1488	1608	1540	1635

Table 3
Brönsted acid sites/Lewis acid sites ratio, obtained from the infrared spectra of pyridine adsorbed on sulfated TiO_2

Samples	Temperature (°C)	Ratio of Brönsted acid sites/Lewis acid sites
1	100	1.4
	200	1.5
	300	1.6
2	100	1.9
	200	1.7
	300	2.7
3	100	1.2
	200	1.5
	300	2.1
3a	100	1.9
	200	2
	300	3.2

ence of a greater number of vacant sites at the surface, in comparison to the rutile crystalline form [22].

The Raman spectra for samples 1 and 2 are very intense, indicating that the samples have a high degree of crystallinity. Comparing the spectra of samples 3 and 3a it can be observed that the latter has more intense bands, indicative of its higher degree of crystallinity, which can be explained by the fact that sample 3a has been calcined which enabled the formation of the anatase phase to a greater extent than in sample 3, which was not calcined.

3.4. Specific surface areas and average pore diameters

The adsorption/desorption isotherms and the graphs of the distribution of the average pore diameters are seen in Figs. 7 and 8, respectively. The results of the specific surface area, volume and average pore diameter, obtained from the BET and BJH analyses are shown in Table 4. All of the samples can be classified as mesoporous materials (pores between 20 and 500 Å).

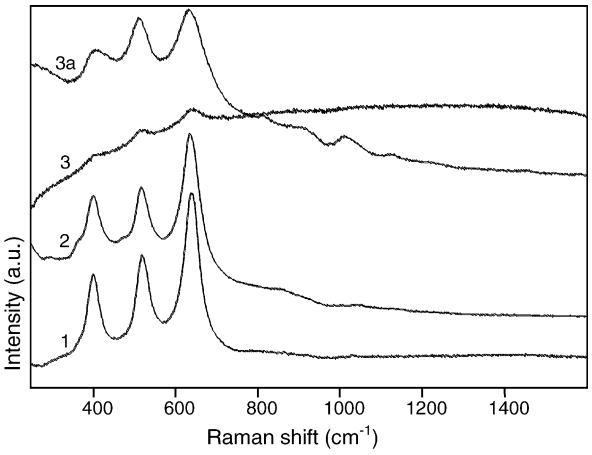

Fig. 6. Raman spectra of samples 1, 2, 3 and 3a, excited by the line at 632.8 nm.

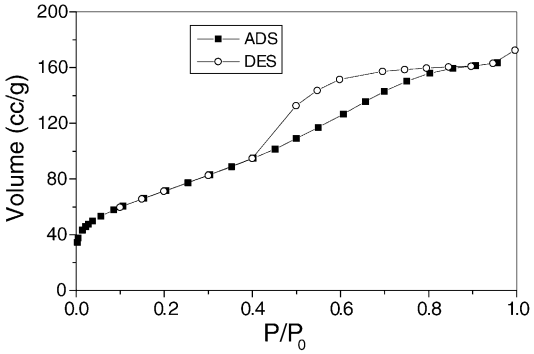

Fig. 7. Adsorption/desorption isotherm.

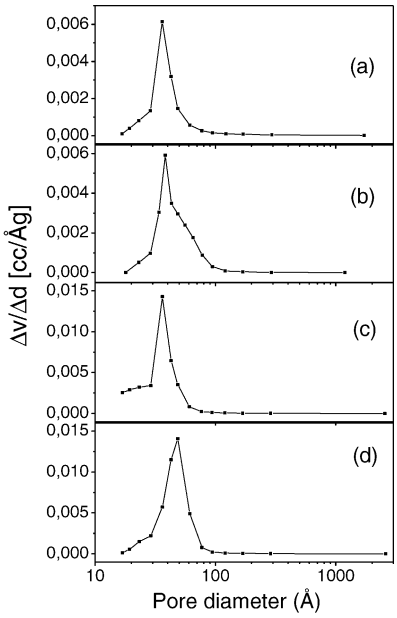

Fig. 8. Distribution of average pore diameters, based on the BJH method: (a) sample 1; (b) sample 2; (c) sample 3 and (d) sample 3a.

The samples with largest specific surface areas are samples 2, 3 and 3a. The sample with the greatest maximum average pore diameter is 3a, however, it is possible to verify that sample 2 has a shoulder, which extents into the pore diameter region above 40 Å, which did not occur with the other samples.

It may be verified that the average pore diameter results show a correlation with the results for the determination of acid sites by infrared spectroscopy. Sample 3a, with the greatest average pore diameter and sample 2, with the greatest

Table 4
Specific surface area and distribution of average pore diameters

Samples	Specific surface area (m^2/g)	Average pore diameter (Å)	Pore volume (cm^3/g)
1	86	36	0.152
2	106	38	0.178
3	256	36	0.266
3a	220	48	0.351

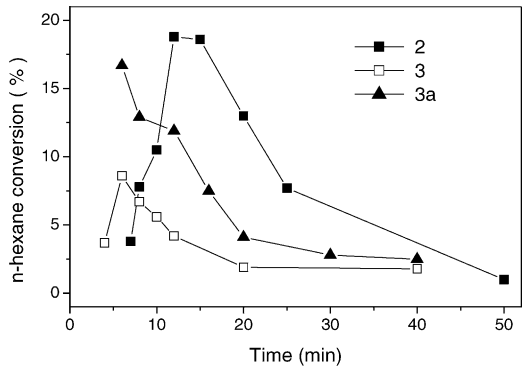

Fig. 9. *n*-Hexane conversion (%) at 100 °C.

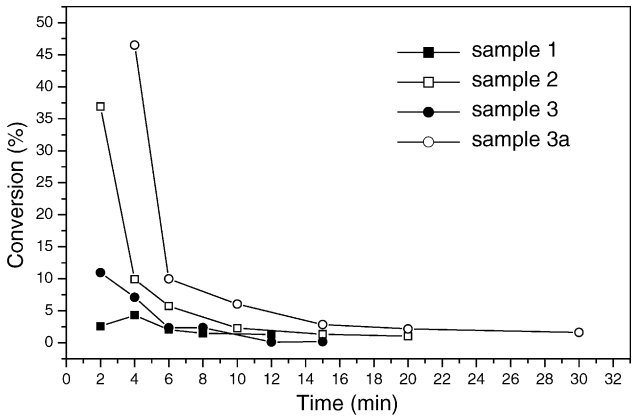

Fig. 10. *n*-Hexane conversion (%) at 200 °C.

concentration of average pore diameters above 40 Å were also the ones which showed a higher ratio of Brönsted acid sites/Lewis acid sites.

3.5. Catalyst tests

3.5.1. n-Hexane isomerization reaction at 100 °C

The conversion of *n*-hexane (%) is shown in Fig. 9. In Table 5 the values for the *n*-hexane conversion and selectivity (%) for the isomerization and cracking products are shown.

It can be seen that the samples which showed higher catalytic activity were samples 2 and 3a, whereas sample 3 showed relatively low activity and sample 1 did not show any activity.

Comparing samples 1 and 2, which differ in the order of H_2SO_4 addition in the material preparation, only sample 2, in which H_2SO_4 was added in the pre-hydrolysis stage, showed activity. Between samples 3 and 3a, which differ in the previous thermal treatment, sample 3a, which was calcinated, showed greater activity.

Comparing the various physical properties measured, it was found that the more active samples (2 and 3a) were those with a greater Brönsted acid site/Lewis acid site ratio and a greater average pore diameter or a concentration of pore diameters above 40 Å. Another interesting fact is that the samples which showed activity (high or low) were those which showed a peak of sulfate loss at a lower temperature (below 600 °C). This latter result indicates that the presence of one type of sulfate, more weakly bound, is necessary, which should be present in a site with higher acidity than the sulfate, more strongly bound, which is lost at a higher temperature. As previously mentioned, similar results have already been observed for sulfated ZrO_2 prepared by the sol–gel method [13] and also for sulfated TiO_2 prepared by impregnation [8].

3.5.2. n-Hexane isomerization reaction at 200 °C

From the graphs of the *n*-hexane conversion (%) (Fig. 10) and the selectivity for isomers and cracking products (Table 6) it is possible to verify that: (i) at a higher temperature all samples showed catalytic activity, even sample 1, which was inactive at a lower temperature, although its activity was very low; (ii) the catalytic activity of all samples investigated increased in relation to the reaction at 100 °C; (iii) despite the activity increase, the selectivity for isomerization decreased, there being a predominance of cracking products at the beginning of the reaction, only with the reaction running does the predominance of isomerization products start for some samples; (iv) samples 2 and 3a continued to be the samples with higher catalytic activity.

Another fact which can be observed is the relatively rapid deactivation, greater than that observed for the reaction at 100 °C, probably due to the deposition of coke, formed from the cracking products. Since at this higher temperature the cracking products predominate at the beginning of the reaction, the formation of coke should also be favored.

Table 5
Conversion and selectivity (%) of sulfated TiO_2 samples for the *n*-hexane isomerization reaction at 100 °C

Samples	*n*-Hexane conversion (%)	Selectivity (%)	
		Isomerization	Cracking
1	–	–	–
2	19	100	0[a]
3	9	100	0
3a	17	100	0

[a] Formation of cracking products during the reaction.

Table 6
Conversion and selectivity (%) of sulfated TiO_2 samples for the *n*-hexane isomerization reaction at 200 °C

Samples	*n*-Hexane conversion (%)	Seletivity (%)	
		Isomerization	Cracking
1	5	30	70
2	37	0[a]	100
3	12	18	82
3a	47	10	90

[a] Formation of cracking products during the reaction.

4. Conclusions

The variations in the preparation of the sulfated TiO_2 catalyst by the sol–gel method caused significant changes in the physico-chemical properties of the catalyst, such as chemical composition, structure, thermal stability, nature of the acid sites, specific surface area and average pore diameter. These properties are of extreme importance to an understanding of the relation between structure and catalytic activity.

The sample that showed the greatest catalytic activity in the *n*-hexane isomerization reaction at 100 °C was that whose preparation involved the addition of concentrated sulfuric acid in the pre-hydrolysis stage. It was found that the thermal treatment of the sample at the highest temperature after preparation, causes an increase in catalytic activity.

In the thermogravimetric analysis the samples which were active showed one of the sulfate loss peaks at around 580 °C.

In the Raman spectra it was observed that all of the samples showed bands characteristics of an anatase crystalline form. The absorbtion spectra in the infrared showed bands attributed to sulfate bound to the metal oxide in the chelate form. In the infrared spectra of adsorbed pyridine the most active samples showed a higher ratio of Brönsted acid sites/Lewis acid sites.

The samples with greater catalytic activity showed a greater average pore diameter 48 Å, or a range of average pore diameter distribution above 40 Å.

The effect of the reaction temperature upon the *n*-hexane conversion and the selectivity for isomerization was also verified. At the lowest temperature, the total conversion is lower, but the selectivity for isomerization is higher.

At the highest temperature, cracking products were the main products, giving rise to the formation of coke, which leads to the more rapid deactivation of the catalyst.

Acknowledgements

Authors acknowledge CNPqCTPetro 2001, CNPq/Edital Universal 2002 and CAPES/Prodoc for supplying the grants and Marly S. Soldi M.Sc. for carrying out the thermogravimetric analysis and Dr. Antoninho Valentini for the specific surface area and average pore diameter analysis. The authors are also grateful to Laboratório de Espectroscopia Molecular (IQUSP, São Paulo) for the use of the BOMEM DA3.16 FTIR and the Renishaw Raman System 3000 and to Professor Oswaldo Sala for the helpful discussions.

References

[1] A. Corma, Chem. Rev. 95 (1995) 559.
[2] L.K. Noda, Quím. Nova 19 (1996) 135.
[3] M. Hino, S. Kobayashi, K. Arata, J. Am. Chem. Soc. 101 (1979) 6439.
[4] M. Hino, K. Arata, J. Chem. Soc. Chem. Commun. 24 (1979) 1148.
[5] G.A. Olah, G.K. Surya Prakash, J. Sommer, Superacids, Wiley, New York, 1985.
[6] F.R. Chen, G. Coudurier, J.-F. Joly, J.C. Vedrine, J. Catal. 143 (16) (1993) 143.
[7] C. Morterra, G. Cerrato, C. Emanuel, V. Bolis, J. Catal. 142 (349) (1993) 142.
[8] L.K. Noda, R.M. de Almeida, N.S. Gonçalves, L.F.D. Probst, O. Sala, Catal. Today 85 (2003) 69.
[9] M. Waqif, J. Bachelier, O. Saur, J.-C. Lavalley, J. Mol. Catal. 72 (1992) 127.
[10] P. Nascimento, C. Akratopoulou, M. Oszagyan, G. Coudurier, C. Travers, J.-F. Joly, J.C. Vedrine, Stud. Surf. Sci. Catal. 75 (1993) 1185 (New Frontiers in Catalysis).
[11] T. Jin, T. Yamaguchi, K. Tanabe, J. Phys. Chem. 90 (1986) 4794.
[12] D. Farcasiu, J.Q. Li, Appl. Catal. A 128 (1995) 97.
[13] D.A. Ward, E.I. Ko, J. Catal. 150 (1994) 18.
[14] H. Armendariz, B. Coq, D. Tichit, R. Dutartre, F. Figuéras, J. Catal. 173 (1998) 345.
[15] I.I. Ivanova, V. Montouillot, C. Fernandez, J.P. Marie, Gilson, Microporous Mesoporous Mater. 57 (2003) 297.
[16] W.N. Delgass, G.L. Haller, R. Kellerman, J.H. Lunsford, Spectroscopy in Heteregeneous Catalysis, Academic Press, New York, 1979.
[17] J.M. Stencel, Raman Spectroscopy for Catalysis, Van Nostrand Reinhold, New York, 1990.
[18] L.K. Noda, Tese de Doutorado, IQUSP, 1998.
[19] L.K. Noda, O. Sala, Spectrochim. Acta A 56 (1) (2000) 145.
[20] J.L. Figueiredo, Catálise Heterogênea, Fundação Calouste Gulbenkian, 1989.
[21] K. Nakamoto, Infrared and Raman Spectra of Inorganic and Coordination Compounds, fourth ed., Wiley, 1986.
[22] I. Carrizosa, G. Munuera, S. Castanar, J. Catal. 49 (1977) 265.